Biomed Microdevices (2012) 14:483–496
DOI 10.1007/s10544-011-9625-4

An implantable MEMS micropump system for drug delivery in small animals

Heidi Gensler · Roya Sheybani · Po-Ying Li · Ronalee Lo Mann · Ellis Meng

Published online: 25 January 2012

Abstract We present the first implantable drug delivery system for controlled timing and location of dosing in small animals. Current implantable drug delivery devices do not provide control over these factors nor are they feasible for implantation in research animals as small as mice. Our system utilizes an integrated electrolysis micropump, is refillable, has an inert drug reservoir for broad drug compatibility, and is capable of adjustment to the delivery regimen while implanted. Electrochemical impedance spectroscopy (EIS) was used for characterization of electrodes on glass substrate and a flexible Parylene substrate. Benchtop testing of the electrolysis actuator resulted in flow rates from 1 μL/min to 34 μL/min on glass substrate and up to 6.8 μL/min on Parylene substrate. The fully integrated system generated a flow rate of 4.72±0.35 μL/min under applied constant current of 1.0 mA while maintaining a power consumption of only ~3 mW. Finally, we demonstrated *in vivo* application of the system for anti-cancer drug delivery in mice.

Keywords Drug delivery · Electrochemical bellows actuator · Implants · Micropump

H. Gensler · R. Sheybani · R. L. Mann · E. Meng (✉)
Department of Biomedical Engineering,
Viterbi School of Engineering, University of Southern California,
1042 Downey Way, DRB-140,
Los Angeles, CA 90089-1111, USA
e-mail: ellis.meng@usc.edu

P.-Y. Li · E. Meng
Ming Hsieh Department of Electrical Engineering,
Viterbi School of Engineering, University of Southern California,
3651 Watt Way, VHE-602,
Los Angeles, CA 90089-0241, USA

1 Introduction

Laboratory animal research plays an essential role in the study and understanding of human diseases. Rats and mice are the most commonly used models and comprise an estimated 95% of laboratory animals used in research (Trull and Rich 1999). The rat was the first mammal domesticated for scientific research, and historically has been preferred over the mouse for physiological and behavioral studies due to the convenience of the rat's larger size and more complex behavior (Benedikz et al. 2009; Petit-Zeman 2004). The mouse, however, has been preferred by geneticists because it is easier to genetically manipulate (Benedikz et al. 2009). Advances in genetic techniques in the rat and improved physiological sampling techniques in the mouse are enabling propagation of both models as a means to better understanding of human disease (Worley et al. 2007). In particular, both rodent models offer a relatively inexpensive way to screen for and investigate the most appropriate delivery of novel therapeutics.

It is well established in the drug delivery literature that both dosage and timing are critical to the study of drug effects on the body (pharmacodynamic responses) (Urquhart et al. 1984; Smolensky and Peppas 2007; Youan 2004), as drug function is often tied to biological rhythms. Chronotherapeutics entails drug therapy that is tuned to biological rhythms which play a role in disease activity and thus impact drug efficacy (Smolensky and Peppas 2007). In treating deep vein thrombosis with the anticoagulant drug heparin, the same dosage can either exceed or fall below the therapeutic level depending on the time of administration (Smolensky and Peppas 2007). Cancer studies have shown that administration of therapy at a particular time in a tumor cell cycle can increase effectiveness while reducing toxicity to normal cells. In the case of diabetes, control over both

basal levels of insulin as well as carefully timed boluses at mealtimes is required in order to mimic natural levels (Youan 2004).

Another important drug delivery parameter is location. Localized delivery, or administration of drug directly to the desired site of action ("site-specific"), is preferred in cases where the drug is intended to act on a specific location and could have serious side effects if delivered systemically (e.g. oral and intravenous routes). Some forms of injection are localized but are undesirable in applications where dosing occurs at high frequency. In some tissues, such as the eye, frequent injection can lead to severe trauma (Ambati et al. 2000). In addition, frequent injection (and related handling) in small animals could induce stress effects that confound study results (Urquhart et al. 1984; Kramer et al. 2001). Localized delivery is not to be confused with "targeted" delivery, which generally refers to molecular systems and nanoparticles that accumulate preferentially at or only act on a specific site, but are actually delivered systemically (Farokhzad and Langer 2009). Some success has been found with these targeted systems, even at the clinical stage, but each drug and carrier molecule combination requires significant laboratory and clinical testing to ensure safety and efficacy. siRNA-based therapies for cancer treatment are one example of an application supporting localized delivery. siRNA has a short half-life *in vivo* (~sec to min). With chemical modification, the half-life can be extended to minutes or days, but at the cost of decreased potency (Dykxhoorn et al. 2006). Having a means of delivering the drug directly to the site of action without delays of systemic administration and without need for chemical modification could provide greater efficacy. In the case of pain management, administration directly to the afflicted site could reduce systemic side effects and decrease the amount of drug required to achieve reduction in pain level (Ruan 2007).

Although there is ample evidence of dose and temporal dependence of drug actions, there are limited means for delivering drugs with control over both dose and timing. The need for localized delivery places further constraints on the method of administration. Conventional drug delivery methods include tether infusion (animal is connected to infusion pump via tether) and vascular access ports (subcutaneously implanted injection ports), but these require frequent handling of laboratory animals and constant care to prevent infection and other complications. As mentioned previously, tethered and restraint-based systems induce stress that may confound study results (Urquhart et al. 1984; Kramer et al. 2001). Implantable pumps offer an alternative to tethered systems, injection ports, and frequent animal handling. However, there are no commercially available implantable pumps suitable for periodic infusion of a drug in small animals (rodents) with control of dosage, timing, and delivery site in chronic experiments. The requirements for this application include: refillability, small size, adjustable flow rate, on/off operation, and low power consumption. For subcutaneous implantation to be a minor procedure, the surgery should involve less than 10% of the animal's surface area (Urquhart et al. 1984). The single-use osmotically-driven Alzet® pumps (Alzet 2011) are of a form factor suitable for use in mice but provide only continuous infusion; the flow rate is predetermined by the water permeability of the pump's semipermeable membrane and is fixed at the time of manufacture. Drug payload lasts from 1 day to 6 weeks and is therefore not adequate for extended chronic studies lasting months. The non-refillable Med-e-Cell Infu-Disk™ (Med-e-cell) is too large for practical implantation in mice (~25 to 30 g), as the smallest available reservoir is 5 mL and weighs ~12 g when empty. The actuation is achieved with an electrochemical cell module that provides only continuous drug delivery at a factory set flow rate. Even at the lowest flow rate, 0.03 ml/h, the maximum delivery duration for the 5 ml reservoir pump is less than a week, making this pump unsuitable for chronic studies lasting longer than 7 days. The Primetech iPrecio® pumps (iPrecio 2011) are programmable prior to implantation, but the regimen cannot be modified afterwards. In addition, this battery-powered pump is too large for use in mice, is single-use only, and the flow rates are limited to a maximum of 30 μL/h.

The issues of controllable delivery in a small platform can be addressed by employing microelectromechanical systems (MEMS) technology, which utilizes fabrication techniques borrowed from the semiconductor industry to produce miniaturized structures, sensors, actuators, and systems. Many MEMS pumps have been reported and are reviewed elsewhere (Nguyen et al. 2002; Laser and Santiago 2004; Woias 2005; Tsai and Sue 2007; Amirouche et al. 2009; Yun and Yoon 2006), but few of these devices feature an integrated reservoir and show feasibility for implantation in small animals. MEMS-based micropumps are generally divided into dynamic (non-mechanical) and displacement (mechanical) types. Non-mechanical micropumps typically are limited in flow rate (maximum of 10 μL/min) (Amirouche et al. 2009), have relatively slow response compared to mechanical micropumps, and often require interaction with a working solution with particular electrical properties, such as conductivity (e.g. electrokinetic pumps) (Laser and Santiago 2004; Tsai and Sue 2007; Amirouche et al. 2009). Examples of dynamic actuation include electroosmosis, electrowetting, electrophoresis, electrohydrodynamics, and magnetohydrodynamics.

Displacement actuation schemes offer distinct advantages for drug delivery applications in small animals, including operation independent of the fluid properties (such as conductivity), higher flow rates, and faster response times (Amirouche et al. 2009). There are numerous displacement-

type actuation methods including electrostatic, piezoelectric, thermopneumatic, shape-memory alloy (SMA), bimetallic, and electromagnetic, and ionic conductive polymer films (ICPF). Of these, piezoelectric pumps are the most common. Smits (1989) described a three piezoelectric valve peristaltic pump designed for insulin delivery. Maillefer et al. presented a piezoelectric ceramic disk-actuated micropump (1999; 2001) that includes a reservoir and battery intended for transcutaneous delivery in humans and weighs over 20 g (Debiotech 2011). Evans et al. (2011) reported an intrathecal drug delivery system with lead zirconate titanate (PZT) valves that consumes low power, but is also intended for human use. Other piezoelectric micropumps have been reported and comparisons between them can be found in (Nguyen et al. 2002; Laser and Santiago 2004; Woias 2005; Tsai and Sue 2007; Amirouche et al. 2009). Piezoelectric pumps offer high forces and fast response times, but disadvantages include high voltage requirements and mounting procedures of PZT disks.

Electrostatic pumps were introduced and demonstrated by Judy et al. (1991) and Zengerle et al. (1992) starting in the early 1990's. Although electrostatic actuation allows fast response times and low power consumption, only small stroke volumes and forces are achieved (Amirouche et al. 2009). In thermopneumatic and phase-change type actuators, large pressures and deflection are achieved, but at the cost of high power consumption, slow response times, and the added fabrication difficulty of a fluid-filled chamber that must be sealed. SMA micropumps feature high deflection, but require high power and special materials. Bimetallic micropumps feature relatively simple fabrication and lower driving voltage, but deflection is small and operation at high frequency is limited (Tsai and Sue 2007). Electromagnetic actuation offers faster mechanical response than thermopneumatic (Woias 2005) and large forces, but suffers from high power consumption, heat generation, and requirement of an external magnet (Woias 2005; Amirouche et al. 2009). In ICPF pumps, applied voltage to metal electrodes deposited on either side of a perfluorosulfonic acid polymer membrane induces bi-directional bending used in pumping. Although there is concern of repeatability issues related to batch fabrication, this scheme boasts low driving voltage, fast response, biocompatibility, and operation in aqueous environments (Tsai and Sue 2007; Amirouche et al. 2009).

In addition to micropumps, there are several passive MEMS drug delivery systems consisting of membrane-sealed microreservoir arrays for controlled release (Santini et al. 2000; Grayson et al. 2003; Li et al. 2004; Elman et al. 2009; Staples 2010). Although microreservoir technology has been demonstrated in acute studies in rats (~150 to 200 g) (Li et al. 2004), there are still some limitations in terms of chronic drug delivery in small animals. Microreservoirs allow for storage and release of one or multiple drugs, but the reservoirs are not refillable. Thus, there must be a compromise between duration of the implant and size of the implant to minimize surgeries for removal and/or replacement of the device. In the case of (Li et al. 2004), membrane dissolution is sensitive to and must be modified for *in vivo* environmental conditions, as protein adsorption affects the gold surface of the membrane and impedes corrosion. The microreservoir seals required a cleaning cycle and at least 10 min of a square wave cycle for the membranes to open consistently.

Despite abundant work in micropumps and drug delivery, there is still an unmet need for localized, controllable delivery in small animals such as mice. Previously, we demonstrated a passive reservoir system (Lo et al. 2009), an electrochemically based system (Li et al. 2008), and an electrochemical bellows actuator (Li et al. 2010) for applications in drug delivery. Lo et al. (2009) reported the development of the first manually-actuated refillable MEMS drug delivery device with an integrated check valve and demonstrated intraocular delivery *ex vivo* in enucleated porcine eyes and *in vivo* in rabbit eyes. Electrolysis was chosen as the actuation method in (Li et al. 2008) for its low power consumption (~μW to mW), low heat generation, large driving force, and flow rate control through adjustment of the applied current (Neagu et al. 1996). An electrochemically driven implantable pump with transscleral cannula (Li et al. 2008) was operated on benchtop and showed a broad operation range (from pL/min to μL/min) and ability to pump against several physiologically relevant backpressures. Feasibility of the electrochemical device for ocular applications was also demonstrated *ex vivo* in enucleated porcine eyes and *in vivo* in rabbit eyes. A Parylene bellows electrochemical actuator introduced by Li et al. (2010) separated the electrolysis operation from the drug reservoir in a benchtop testing fixture and achieved large deflection under low power. Various electrode geometries were investigated to optimize pump performance in terms of gas generation and efficiency.

Here we present, for the first time, a refillable implantable micropump system (RIMS) with an integrated electrochemical bellows actuator in a form factor suitable for use in small animals (e.g. rodents). RIMS provides repeatable, controllable drug delivery to a specific site. The system is made of biocompatible materials, has a refill port, and features an inert drug reservoir to enable broad drug compatibility. Our fully implantable system is capable of adjustment to the delivery regimen while implanted, a feature not available in commercial devices on the size scale of our system. With the adjustability in flow rate offered by our system, a multitude of pharmacodynamic responses can be studied in a way that has not been possible until now. We also demonstrate, for the first time, an implantable MEMS micropump system for controlled dose, timing, and location of drug delivery in mice.

2 Design

The bellows electrolysis actuator consists of a pair of interdigitated platinum (Pt) electrodes contained within a bellows filled with electrolyte (water). Electrical current applied to the electrodes splits the water molecules into hydrogen and oxygen gases (Fig. 1). The bellows expands under the imposed pneumatic driving force of the gases generated by the electrolysis reaction, which then pushes the fluid (drug) surrounding the bellows out of the reservoir and catheter to the delivery site. When the current is turned off, the Pt electrode acts as a catalyst for the gases to recombine as water (Li et al. 2010). The electrolysis actuator can be set to on/off states and provide adjustable flow rate (through applied current magnitude) to achieve a desired delivery regimen. Our actuation method allows multiple dosing cycles, which combined with a refillable reservoir, makes our RIMS appropriate for chronic use.

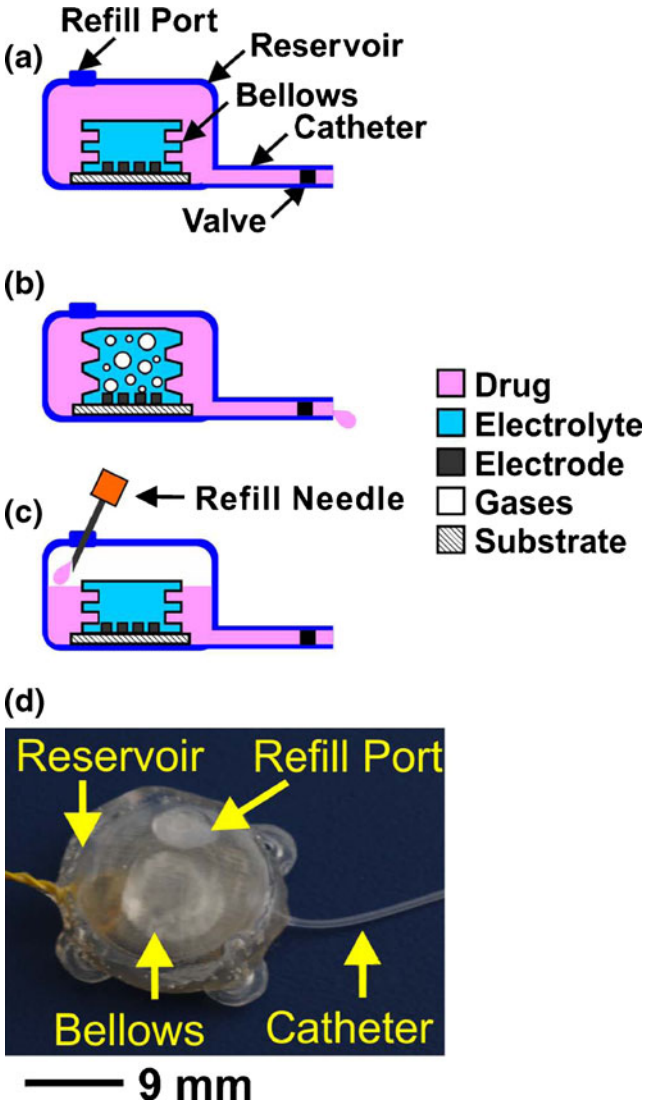

Fig. 1 Illustrations and photograph of the refillable implantable micropump system (RIMS) (**a**) The main features are an electrochemical bellows actuator, refill port, and check valve (**b**) Current applied to a pair of interdigitated electrodes splits water (electrolyte) into hydrogen and oxygen gases. The phase change induces a pressure increase within the bellows and drives fluid out of the reservoir and through the catheter (**c**) The reservoir can be refilled through the built-in refill port (**d**) Photograph of the RIMS

Pt was chosen as the electrode material due to its biocompatibility, role as the catalyst for recombination, and its resistance to oxidation and corrosion (Meng et al. 2008). The interdigitated electrode design was chosen to reduce the resistive path through the electrolyte, which translates to improved efficiency and lower heat generation (Belmont and Girault 1994). The dimensions of the electrode features (100 μm wide interdigitated fingers, 100 μm spacing) were chosen based on improved robustness seen with increased finger width. In consideration for a drug delivery reservoir implanted next to a rounded body feature, such as the eye, it is desirable to have a flexible electrode substrate that coupled with a curved reservoir design so as to better conform to the anatomy of the implantation site (Lo et al. 2009; Li 2009). To this end, we investigated Parylene C as a flexible substrate material. Electrodes on glass substrate were ~8 mm in diameter in terms of overall footprint, but the electrodes on Parylene C were fabricated with a smaller overall diameter of ~4 mm due to the intended application in the eye (less space for implantation).

A bellows actuator format (Li et al. 2010) was adopted to separate the drug from the electrolyzed fluid and prevent associated drug oxidation, an undesirable effect reported in our previous work (Li et al. 2009). Parylene C was selected as the bellows material for its biocompatibility, inertness, very low permeability, and low Young's modulus to achieve high deflections with low applied pressure. A flexible bellows configuration was chosen over corrugated or flat membranes for their higher deflection with lower material stress under pressure loading (Li et al. 2010). The dimensions of the bellows were chosen based on the size of the electrodes and the height of the reservoir. The bellows volume occupies significant space within the reservoir and therefore its dimensions must be appropriately selected to minimize dead volume while still maintaining the ability to deliver sufficient drug volumes. A bellows with 2 convolutions was chosen over 1 and 3 convolutions to balance the requirements of deliverable volume against dead volume and overall device dimensions (Gensler et al. 2011).

The drug reservoir was made of biocompatible silicone rubber, chosen for its ease and low cost of fabrication, and has rounded features to reduce irritation and erosion of tissue around the implanted system. The dimensions were chosen based on bellows actuator dimensions and constraints on total implanted volume due to the use in small animals, and can be easily modified for different applications. For subcutaneous implantation to be a minor procedure, less than 10% of the animal's surface area should be involved in the creation of a subcutaneous pocket (Urquhart

et al. 1984). The catheter material was biocompatible silicone rubber and its dimensions were chosen to minimize flow resistance while taking into consideration placement in the animal. This was in contrast to the Parylene cannula used earlier in (Li et al. 2008), which had clogging issues, was not robust enough to withstand surgical handling and implantation (kinking), and did not include an in-line valve. The silicone rubber catheter here has a larger, circular cross section to avoid clogging.

Integration of a check valve in the drug delivery catheter ensures safe dosing as well as separation of the reservoir contents from fluids at the implantation site (Lo and Meng 2009). The integrated check valve described in (Lo et al. 2009) had a relatively high cracking pressure (~10 kPa or 76 mmHg) and was integrated into a rectangular cannula, which is difficult to secure and seal with sutures. Here we chose to use an in-line check valve with high pressure shutoff as previously described (Lo and Meng 2009, 2011). The valve was designed to open at low forward pressures during drug delivery, but to be closed under back pressure and at excessive forward pressures greater than a preset threshold to prevent accidental dosing under pump malfunction or other unexpected conditions.

3 Methods and materials

3.1 Electrodes

3.1.1 Fabrication

Previously we described a dual-layer photolithography and liftoff process for platinum (Pt) electrode fabrication on a glass substrate (Li et al. 2010) and flexible Parylene C substrate (Li 2009; Gensler et al. 2010) (Fig. 2). An undercut formed on the photoresist sidewall assisted with metal liftoff. A soda lime wafer was treated with 1,1,1,3,3,3-hexamethyldisilazane (HMDS, MP Biomedicals, LLC, Solon, OH) for improved adhesion between the wafer and photoresist. A layer of photoresist (AZ1518, AZ Electronic Materials, Branchburg, NJ) was spun onto the treated soda lime wafer at 4 krpm for 30 s and globally exposed at 90 mJ/m^2. A second layer of photoresist (AZ4400, AZ Electronic Materials, Branchburg, NJ) was spun on at 4 krpm for 30 s and UV patterned with 90 mJ/m^2. After descumming for 60 s in oxygen plasma (100 mW, 100 mTorr), Pt (2,000 Å) or Pt/Ti (2,000 Å/500 Å) electrodes were deposited by e-beam evaporation. Ti acted as an adhesion layer between the Pt and glass. Electrodes (100 μm wide interdigitated fingers, 100 μm spacing) were then defined by standard liftoff by immersion in acetone, isopropyl alcohol, and deionized water. Kynar™ wire-wrap wires (30 AWG, Jameco Electronics, Belmont, CA) were affixed to electrodes using conductive epoxy (Epo-tek® H20E, Epoxy Technology, Billerica, MA), and further coated with non-conductive epoxy (5-Minute Epoxy System, ITW Performance Polymers, Riviera Beach, FL) for insulation.

For the electrodes on Parylene C, a silicon wafer (supporting substrate used only during processing) was coated with 5 μm Parylene C (Specialty Coating Systems, Indianapolis, IN). Native oxide was not removed prior to coating in order to facilitate release of the Parylene C from the silicon support. The photolithography and liftoff steps were the same as those for the glass electrodes. Electrodes were cut with a razorblade and peeled from the supporting Si substrate, then mounted with epoxy (5-Minute Epoxy System, ITW Performance Polymers, Riviera Beach, FL) on a flexible polyetheretherketone (PEEK) backing for subsequent packaging.

3.1.2 Characterization

Electrochemical impedance spectroscopy (EIS) is an electrochemical technique where the application of current or voltage across a broad range of frequencies can provide information about electrochemical reactions and characteristics of the electrode. EIS can be used to study surface changes due to corrosion, effects of dielectric coatings, electrochemical cleaning, surface activation, or electrolytic solution conductivity (Parthasarathy 1992; Bard 2001; K'Owino and Sadik 2005). We performed potentiostatic EIS (voltage potential between working and reference electrode kept constant) and measured the current value between the working and counter electrodes, which was then used to plot impedance as a function of frequency. The change in shape of the impedance curve for an electrode before and after the electrode has been used in electrolysis provides insight on the status of the electrode surface, indicating, for example, whether corrosion or delamination have occurred. Electrodes were characterized using EIS (Gamry Reference 600 Potentiostat and EIS300 Software, Gamry Instruments, Warminster, PA) performed in 1X phosphate buffered saline before and after application of current. 0.2, 0.6, and 1.0 mA were applied successively to the same Pt/Ti electrodes on Parylene C, and additionally at 10.0 mA for electrodes on glass.

Electrodes were fixed in a custom laser-machined (Mini/Helix 8000, Epilog, Golden, CO) acrylic test fixture filled with deionized water. The application (2 min) of constant current (2,400 Sourcemeter, Keithley, Instruments Inc., Cleveland, OH) induced electrolysis, which split water into hydrogen and oxygen gases. This phase change was accompanied by an increase in pressure, which then dispensed the fluid through the fixture output and into a small weigh boat (measured with a 1 mg-resolution digital balance) for volumes >100 μL or into a calibrated micropipet (Accu-Fill 90, Becton, Dickinson and

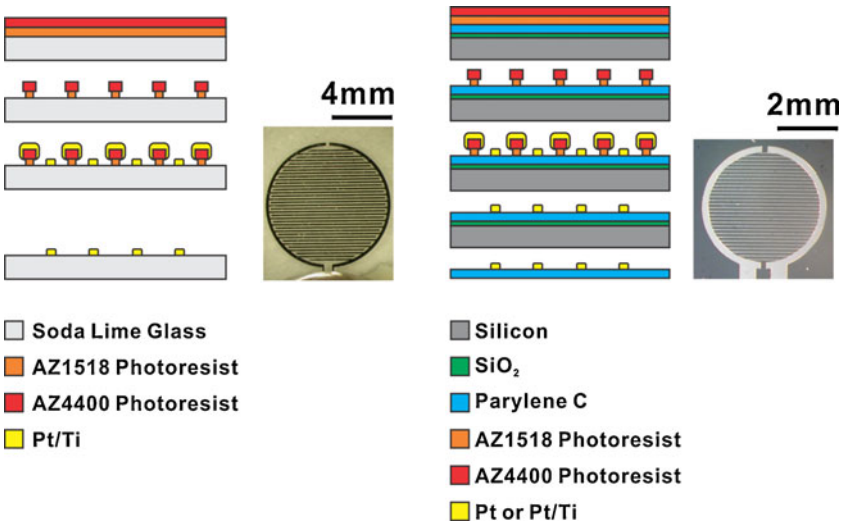

Fig. 2 The dual-layer photoresist process for electrode fabrication on glass (*left*) or Parylene C (*right*, photograph taken prior to detachment from silicon support)

Company, NJ) for delivered volumes <100 μL. Electrodes on glass were tested from 1.0 mA to 5.0 mA and electrodes on Parylene C were tested from 0.2 mA to 2.0 mA (Fig. 3).

3.2 Bellows

Parylene C bellows with 2 convolutions were fabricated using a polyethylene glycol (PEG 1,000 Mn, Sigma-Aldrich, St. Louis, MO) molding process described previously (Li et al. 2010; Gensler et al. 2011). The process used here and in (Gensler et al. 2011) improved upon the process developed for (Li et al. 2010). The silicone rubber molds in the new process are reusable and several steps were eliminated to significantly reduce the time required for the molding process from 1 week to 1 day. Additionally, the Mn of PEG was reduced from 14,000 to 1,000 in order to obtain smoother and less brittle PEG forms. The process began with punching 9 and 6 mm holes in 0.4 mm thick silicone rubber sheets (10:1 base-to-curing agent ratio Sylgard 184, Dow Corning, Midland, MI). These were then layered on glass slides as shown in Fig. 4 to form modules. Each module was filled with molten (~50°C) PEG, taking care to ensure that no air bubbles were introduced to the molds. After several minutes at room temperature the PEG was solidified and the silicone molds were peeled away, leaving solid PEG modules that could be stacked to form the final 2 convolutions PEG form. The modules were fused together by slightly moistening the appropriate water-soluble PEG faces of each module with water. A 13.5 μm layer of Parylene C (Specialty Coatings Systems, Indianapolis, IN) was deposited over the PEG form, and then the PEG was dissolved out of the bellows by soaking in water at room temperature.

Load-deflection tests were performed on a 2 convolution Parylene C bellows (13.5 μm wall thickness). Bellows were mounted in a custom laser-machined (Mini/Helix 8000, Epilog, Golden, CO) acrylic test fixture and pressures ranging from 0.0 psi to 0.5 psi (3.45 kPa) were applied in increments of 0.05 psi (0.34 kPa) using a computer-controlled pressure regulator (900X, ControlAir, Inc.,

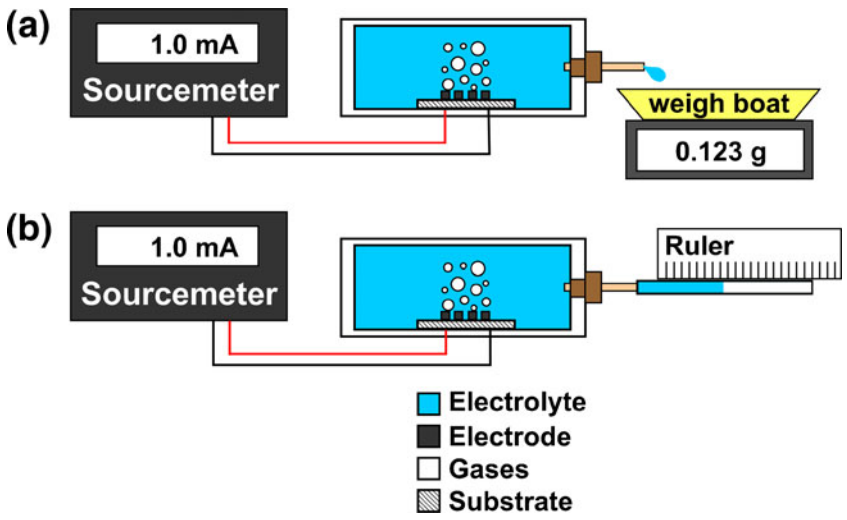

Fig. 3 A sourcemeter provided current to the electrodes for electrolysis in a testing fixture, then fluid was dispensed into (**a**) a weigh boat for volumes >100 μL or (**b**) a calibrated micropipet for volumes <100 μL

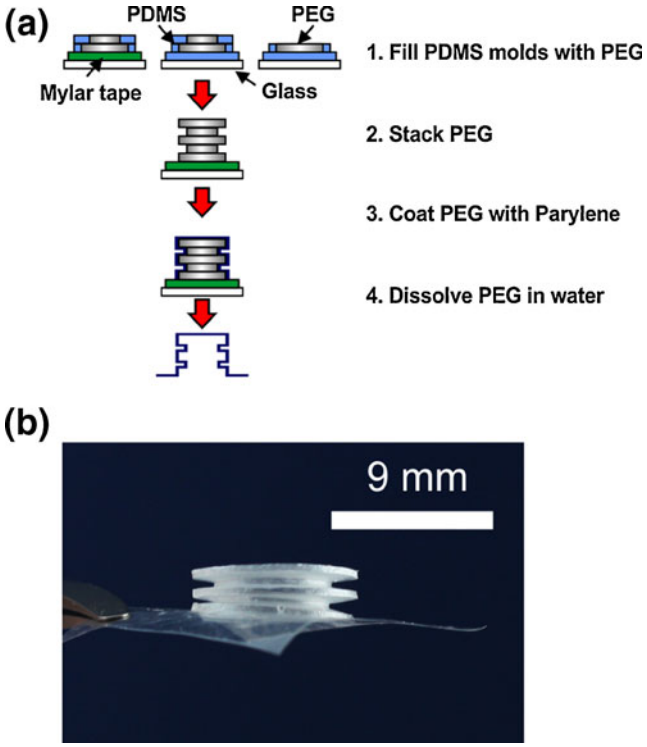

Fig. 4 (**a**) Fabrication of the bellows consisted of molding a PEG form using PDMS, deposition of Parylene C over the PEG mold, and removal of the sacrificial PEG (**b**) Photograph of the 2 convolution Parylene C bellows after removal of PEG

Amherst, NH). Deflection was recorded using a compound microscope (PSM-1000, Motic China Group Co., Xiamen, China) with a 100× objective lens (1 μm vertical resolution).

The Parylene C bellows was filled with room temperature deionized water and adhered to the electrode substrate with double-sided pressure sensitive adhesive film (Tape 415, 3M, St. Paul, MN). The seal was further reinforced with epoxy (5-Minute Epoxy System, ITW Performance Polymers, Riviera Beach, FL). After assembly of the bellows and the electrode, the bellows actuator was mounted in the same fixture for stand-alone electrodes and flow rates were measured at currents ranging from 0.2 mA to 1.0 mA (Li et al. 2010).

3.3 MEMS check valve

The four-part MEMS check valve (Lo and Meng 2011) consisted of a valve seat, pressure limiter, and spacer plate made of SU-8 2100 (MicroChem, Newton, MA), and an s-shaped arm valve plate made from MDX-4-4210 (10:1 base-to-curing agent ratio, Dow Corning, Midland, MI). The components were aligned and held in a custom fixture and covered with 1.3:1 shrink ratio fluorinated ethylene propylene (FEP) heat-shrink tubing (22 G, Zeus Industrial Products Inc., Orangeburg, SC). The entire fixture assembly was placed in a vacuum oven (Model V0-914A Lindberg Blue, Asheville, NC) and heated at a rate of 1.5°C to 215°C, the temperature for the heat shrink process recommended by the FEP tubing manufacturer. After 30 min of baking, the temperature was ramped down at a rate of 1.5°C to avoid thermal stress on the SU-8. The FEP tubing shrank to hold the valve components securely without the need for adhesives (Fig. 5). The outer diameter of the valve and FEP packaging was ~1.23 mm, which is significantly smaller than either of the commercial valves and allows integration into the system without significantly adding to the overall device size.

The valve was characterized with a custom pressure setup. Pressurized water was applied to the inlet of the valve incrementally from 0 kPa to 266.62 kPa (2,000 mmHg or 38.67 psi). Flow rate was measured in a calibrated micropipet (Accu-Fill 90, Becton, Dickinson and Company, NJ) attached to the valve outlet. The valve was kept dry prior to the first application of pressurized water, but was submerged in water before the second run to prevent stiction, which was observed previously and described in (Lo and Meng 2011).

The MEMS check valve was compared to two commercial valves (Fig. 6) using the same pressure setup. The first was a one-way disc valve (240270524, Halkey Roberts, St. Petersburg, FL) constructed of a Class VI biocompatible polycarbonate housing and silicone seal disc and chosen for its low cracking and sealing pressures (<0.25 psi or 1.72 kPa and ≤0.50 psi or 3.45 kPa, respectively, according to manufacturer). The second, a normally closed in-line check valve (80031, Qosina, Edgewood, NY) made of acrylic and ethylene propylene diene monomer, has an even lower cracking pressure of <0.05 psi or 0.35 kPa according to the manufacturer.

3.4 Refillable Implantable Micropump System (RIMS)

Rapid prototypes of the reservoir were made using silicone rubber casting in custom CNC milled acrylic molds. Medical grade silicone rubber (MDX-4-4210, Dow Corning,

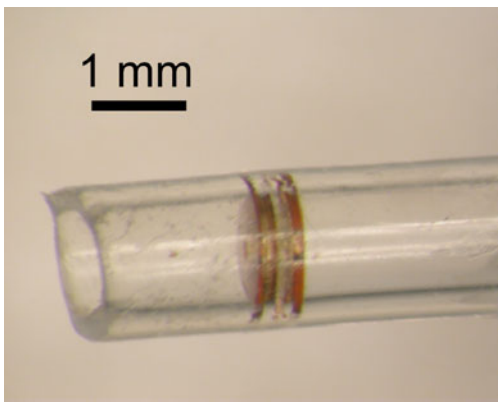

Fig. 5 Side view of the check valve packaged in FEP tubing

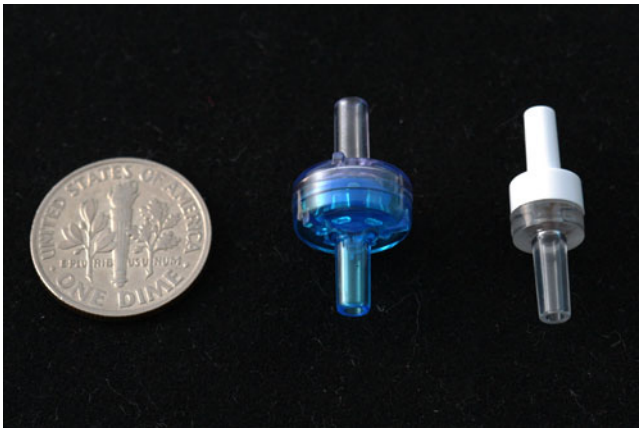

Fig. 6 Commercial one-way disc valve (*left*) and in-line check valve (*right*) used for comparison to the fabricated check valve

Midland, MI) was thoroughly mixed (Super Mixer AR-250, Thinky Corp., Tokyo, Japan) in a 10:1 base-to-curing agent ratio and then degassed in a vacuum chamber (Model V0-914A Lindberg Blue, Asheville, NC) for 45 min. The uncured solution was poured into the molds and baked in an oven (EC0A Environmental Chamber, Sun Electronic Systems Inc., Titusville, FL) for approximately 1 h at 80°C to cure the polymer. Class VI silicone tubing (VWR International, Radnor, PA) was set in the mold during curing. A slot was made on the back reservoir wall for inserting the bellows actuator. A small amount of uncured MDX-4 was used to adhere the bellows actuator to the inner base of the reservoir and seal around the slit and lid of the reservoir. The fully packaged device (Fig. 7) was then cured at 80°C for approximately 45 min. A 30-gauge non-coring needle was used to fill the reservoir with deionized water for testing as previously demonstrated (Lo et al. 2009).

The FEP-packaged valve inlet was connected to the integrated silicone catheter and its outlet was connected to a calibrated micropipet as previously described for bellows actuator testing. Constant current of 1 mA was applied (2400 Sourcemeter, Keithley Instruments Inc., Cleveland, OH) for 15 min, then turned off for 45 min. This on/off cycle was repeated four times for both valved and non-valved systems to simulate periodic dosing in a chronically implanted device. For all of the valved systems, valves were soaked overnight in water prior to testing. The commercial valves were each connected to the outlet of the RIMS catheter in place of the integrated MEMS check valve and tested similarly.

4 Results

4.1 Electrodes

EIS was performed on electrodes on glass and Parylene C substrates before and after the application of constant current. As expected for two metal (reference and working) electrodes in solution, the overall impedance trend decreases with increasing frequency in all cases (Fig. 8). For electrodes on glass, after the first application of current, the impedance decreases at all frequencies and exhibits only slight change for increasing current. The first application of current (0.2 mA in this case) acts as a cleaning cycle (Sawyer 1974, p.78) that increases the effective active surface area of the Pt catalyst, which can be seen in the impedance shift after the application of 0.2 mA in Fig. 8. The electrode surface becomes more active and stabilizes upon the first application of current. This change does not cause any significant effect on the flow rate in the first versus subsequent tests. Electrodes on glass were able to withstand up to 10.0 mA of current without any degradation. Stand-alone electrodes were tested at the benchtop prior to integration with reservoirs. A broad range of current-dependent flow rates was successfully demonstrated. Constant currents from 1.0 mA to 5.0 mA applied to Pt/Ti electrodes on a glass substrate resulted in flow rates from ~1 μL/min to 34 μL/min, respectively, in an approximately linear relationship (Li et al. 2010).

Pt electrodes on Parylene C, however, delaminate even for modest (>1 mA) applied currents (Fig. 9). The dimensions and surface area of the electrodes on glass were larger than those of electrodes on Parylene C, thus the impedance magnitudes of the EIS should not be directly compared. However, the overall (and expected) trend of decreasing impedance with increasing frequency was also present for the electrodes on Parylene C.

Electrodes on Parylene having a Ti adhesion layer were also fabricated and a subset were annealed (205°C). There is evidence that annealing may help stabilize Ti-polymer interfaces (Faupel et al. 1998). However, we found that at currents above 1 mA delamination was delayed, but not prevented, for Pt-Ti electrodes on Parylene C following annealing (at 150 and 205°C) and a more aggressive descum prior to metal deposition. With annealing, electrode delamination occurred on the order of seconds. Overall, the greatest improvement in electrode adhesion under applied current was attained by inclusion of the Ti adhesion layer but without subsequent annealing of the metal/Parylene C composite film (Fig. 10). For electrodes on Parylene with the Ti adhesion layer but no annealing, electrodes did not show delamination for up to 30 min at constant current less than 1 mA. Above 1 mA, signs of degradation occurred in less 10 min.

4.2 Bellows and bellows actuators

Load-deflection tests were performed on a 2 convolution Parylene C bellows (13.5 μm wall thickness) as described in (Gensler et al. 2011) and a typical result is shown in Fig. 11. A deflection of approximately 1.08 mm was achieved at

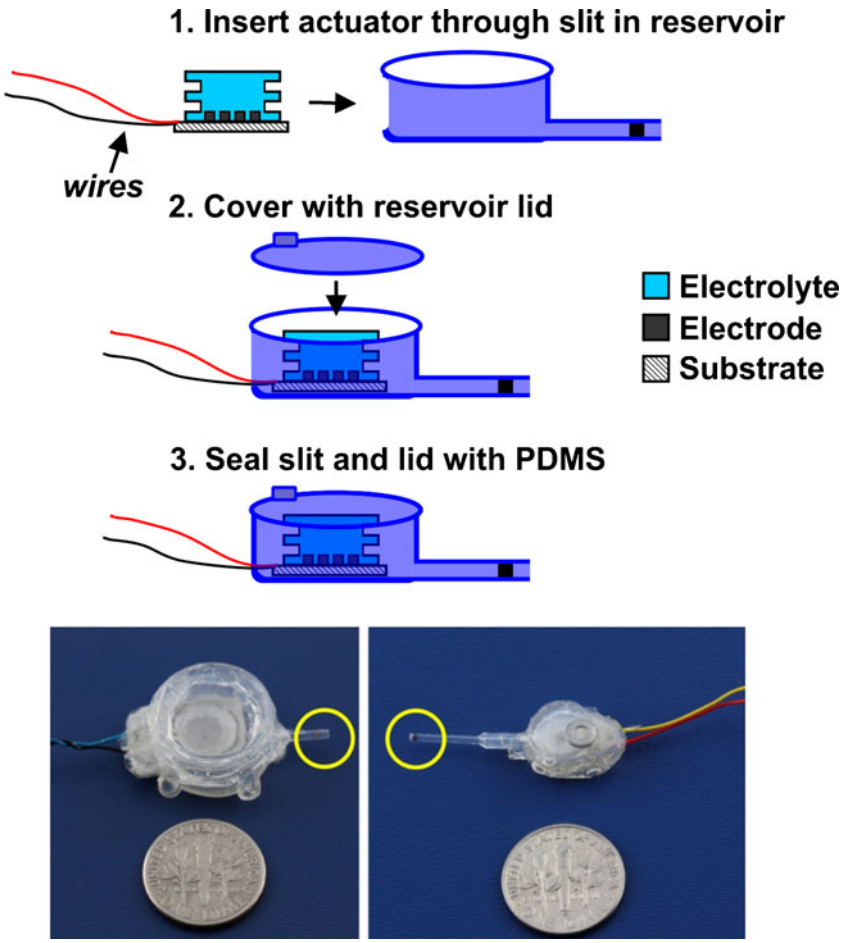

Fig. 7 Assembly of the RIMS. The bellows actuator is inserted into the cast silicone rubber reservoir, then PDMS is used to seal the slit and adhere a lid to the reservoir. Photograph (*bottom*) of the MEMS check valve integrated with the fully packaged micropump system (*left*) and a miniature prototype (*right*)

3.45 kPa (25.85 mmHg or 0.5 psi), demonstrating large deflection under relatively low applied pressure. This is in comparison to the bellows with a 10 μm wall thickness described in (Li et al. 2010), which deflected 1.78 mm at 3.45 kPa. Deflection followed a nonlinear relationship with wall thickness, decreasing for thicker walls, and increased with additional convolutions. The deflection exhibited a cubic relationship with pressure and at 13.5 μm operates within the elastic region for our pressure range (Gensler et al. 2011). Plastic deformation for 13.5 μm wall thickness typically occurs above 6.89 kPa (51.71 mmHg or 1.0 psi). Bellows were then adhered to glass electrodes and tested similarly to the stand-alone electrodes at currents between 0.2 and 1.0 mA, and demonstrated a linear relationship with flow rate (Li et al. 2010), which was consistent with our previous observations. An additional test was performed to determine the maximum deliverable volume before bellows failure (leaks or pops). For a 2 convolution bellows of 13.5 μm wall thickness, the maximum deliverable volume was 228 μL and was set to provide a safety margin to prevent plastic deformation of the Parylene C bellows.

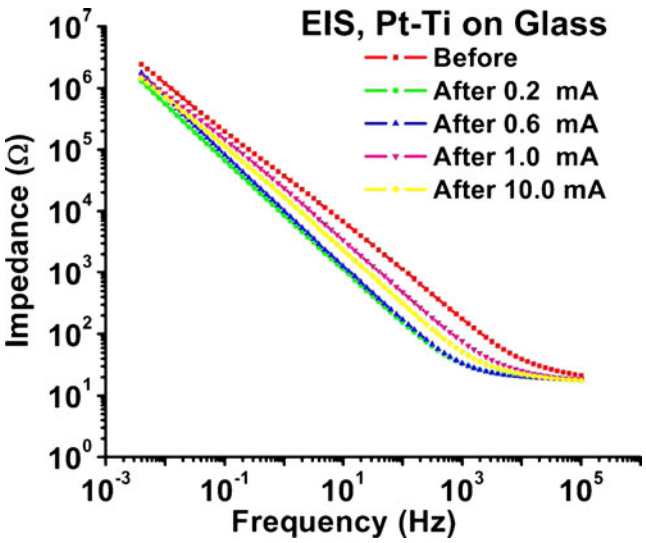

Fig. 8 EIS results of electrodes on glass show an overall decrease in impedance with increasing frequency, as expected for two metals electrodes (reference and working) in solution

4.3 MEMS check valve

The check valve cracking pressure was approximately 1.31 kPa (9.82 mmHg or 0.19 psi) and the (forward) closing pressure 93.29 kPa (699.64 mmHg or 13.53 psi). The valve remained closed and no leaks were observed up to the highest

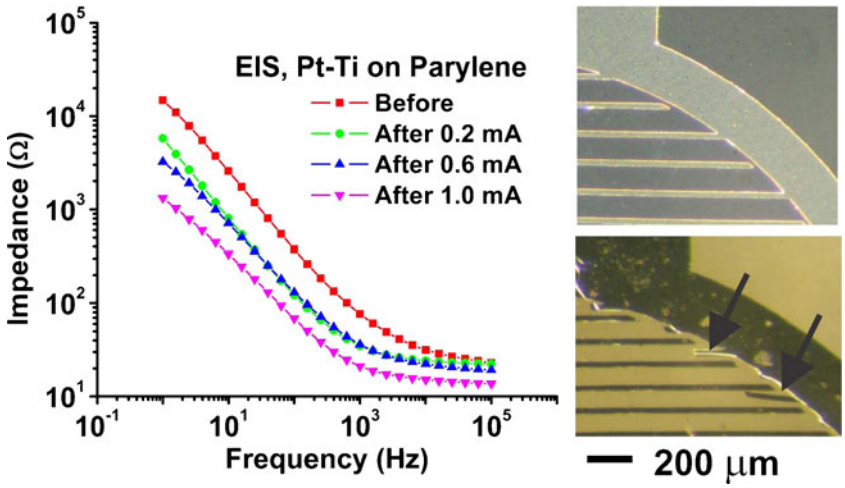

Fig. 9 EIS results of electrodes on Parylene show an overall decrease in impedance with increasing frequency, as expected for an electrochemical cell. Delamination was seen above 1 mA for Pt-Ti electrodes deposited on a Parylene C substrate. As fabricated (*top right*) and delaminated (*bottom right*) electrodes

forward pressure tested at 266.62 kPa (1999.63 mmHg or 38.67 psi). Keeping the valve hydrated did not significantly change the cracking pressure, but the (forward) closing pressure of the valve increased. The MEMS check valve was compared to two commercial valves and the cracking pressures are shown in Table 1.

4.4 Refillable implantable micropump system

Constant current of 1.0 mA was applied for 15 min to bellows actuators (Pt/Ti electrode on glass, 2 convolution bellows) in a non-valved and three valved versions of the RIMS. The duration of current application was based on total dose requirements and desired flow rate for a specific application of the system in radiation dose reduction in cancer. The system had a power consumption of ~3 mW when operated at 1 mA. Current was turned off for 45 min in between delivery periods to allow recombination to occur and the bellows to deflate. The non-valved RIMS (Fig. 12) produced a flow rate of 4.72±0.35 (mean ± SE, n=4) μL/min with current ON. There was an approximate 5-minute delay until significant positive fluid flow for the non-valved RIMS. When the current was removed, the gases recombined and the bellows deflated. Without a valve and with the outlet of the catheter (or micropipet) exposed (to air or an uncovered container with liquid), fluid moved along the catheter in reverse towards the reservoir. Even after recombination had ceased, the position of the fluid in the catheter did not fully return to the original starting location.

Neither of the commercial valves nor the MEMS check valve fully prevented backflow during the recombination

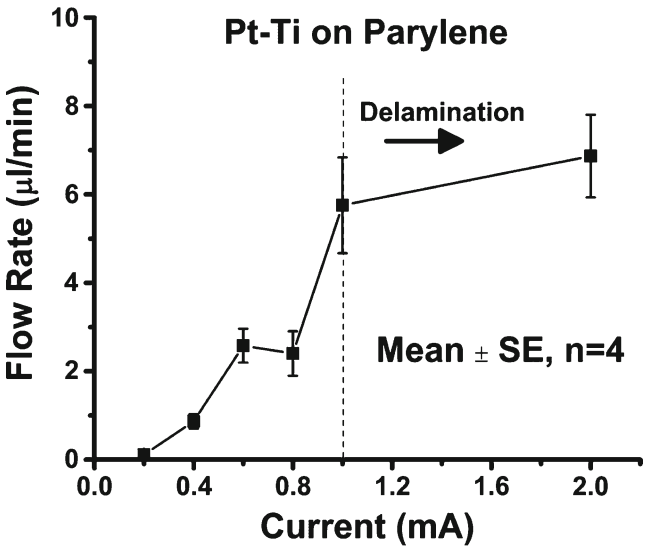

Fig. 10 Flow rates (mean ± SE, n=4) for Pt/Ti electrodes on a Parylene C substrate show higher variability than those on glass and exhibit delamination, particularly at currents above 1.0 mA

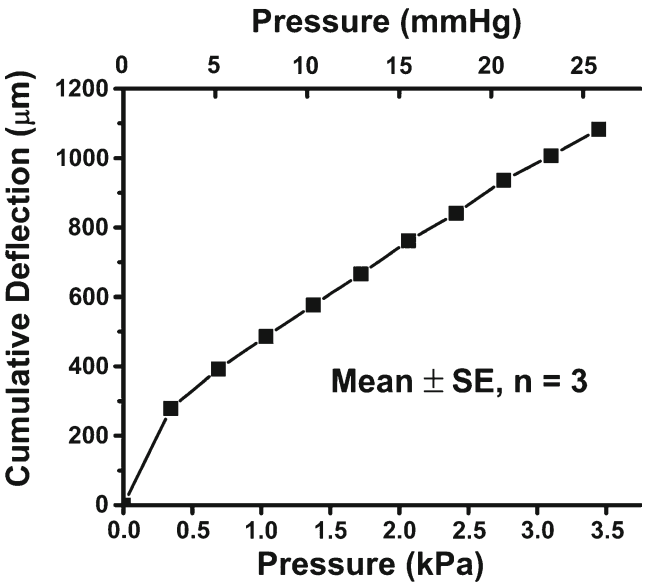

Fig. 11 Load-deflection results for a 2 convolution, 13.5 μm wall thickness bellows under applied pressure

Table 1 Comparison of valve cracking pressures

Valve	Cracking pressure (psi / kPa / mmHg)
MEMS check valve	0.19 / 1.31 / 9.82
One-way disc valve	<0.10 / 0.690 / 5.17
In-line check valve	<0.05 / 0.345 / 2.59

period (Fig. 13). The delay to forward flow in the RIMS with a valve was only slightly longer (seconds) than the non-valved RIMS, but the valves added resistance to the flow path. Flow rates were slightly reduced to 4.28 μL/min (MEMS check valve), 4.67 μL/min (one-way disc valve), and 4.49 μL/min (in-line check valve). In all cases, the fluid front in the catheter flowed in reverse during recombination, but did not return completely to the original starting position.

5 Discussion

Electrode delamination was one of the primary concerns for the system's electrochemical actuator when fabricated on the flexible polymer substrate. Three electrode fabrication methods were investigated for the polymer substrate case: Pt on Parylene, Pt-Ti on Parylene, and Pt-Ti on Parylene with annealing. We found that a Ti adhesion layer without subsequent annealing resulted in the most robust electrodes on Parylene C substrate, but for higher and longer durations of applied current delamination was still observed. General mechanisms for metal-polymer adhesion are physisorption due to Lifshitz-Van der Waals forces, molecular interactions, chemical interaction, and electrostatic interaction (Faupel et al. 1998; Lee 1991). Improved adhesion with a Ti adhesion layer is likely due to double bonds that form between Ti and carbon in the Parylene C as suggested in (Vasenkov 2011). Lee et al. (2004) demonstrated that annealing increased crystallinity in Parylene C films and led to improved adhesion to Au. Wu et al. (1996), however, found conflicting results and attributed decreased adhesion after annealing to two possible mechanisms: the thermal stress induced by a difference in the coefficients of thermal expansion (CTE) between Parylene N (44–69 ppm/K) and Cu (16.6 ppm/K), and phase separation that transforms the intermixed interfacial layer (Parylene and metal) into an abrupt interface. In our experience, annealing did not improve adhesion of Pt-Ti to Parylene. For Pt electrodes on Parylene without the adhesion layer, some improvement in adhesion was seen with annealing at 205°C. Parylene C has a CTE of 35 ppm/K, whereas Pt and Ti have a CTE of 8.8 ppm/K and 8.4–8.6 ppm/K, respectively.

The bellows prevented the drug from being affected by the electrolysis reaction, but did not significantly impede actuation. We previously reported that varying the bellows convolution number (and thus bellows volume) (Sheybani et al. 2011) did not significantly affect actuator performance in terms of flow rate. Recombination is essential to being able to deliver multiple drug boluses, because the bellows should only be operated within the limit of plastic deformation.

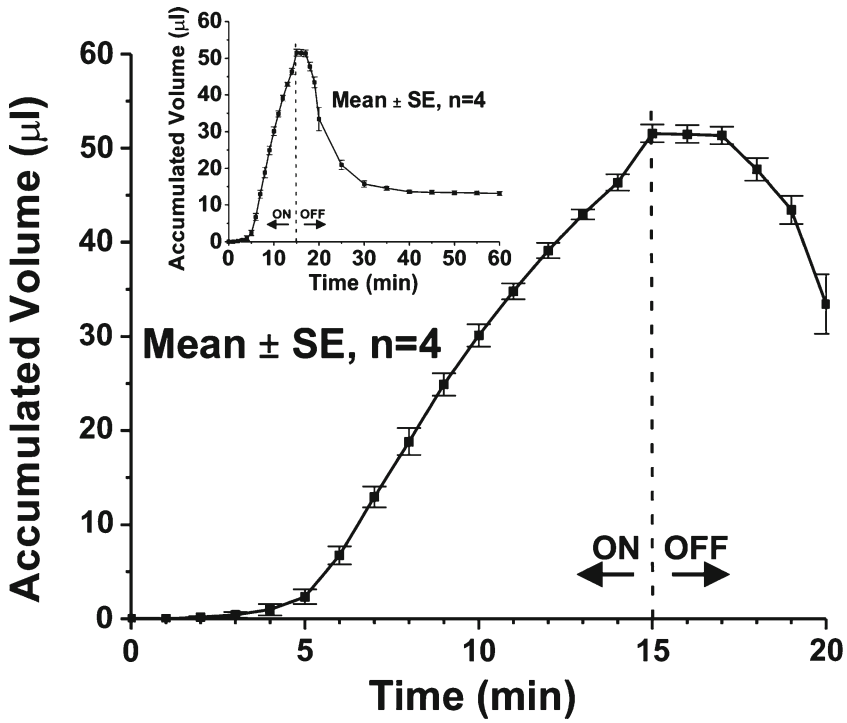

Fig. 12 Constant current of 1.0 mA was applied for 15 min and turned off for 45 min for 4 cycles in a RIMS with no valve. After current was removed, and without a valve, a significant portion of the delivered volume flows in reverse during recombination (*inset*)

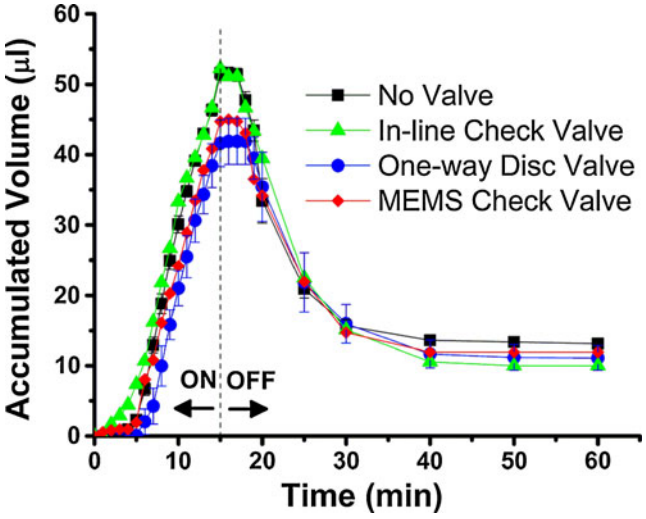

Fig. 13 Constant current of 1.0 mA was applied for 15 min and turned off for 45 min in a RIMS with no valve (n=4 consecutive runs), a commercial one-way disc valve (n=4 consecutive runs), a commercial in-line check valve (n=1), and a MEMS check valve (n=1)

After determining the most robust electrode fabrication process, the actuator with electrolyte-containing bellows was integrated into the drug reservoir. Electrolysis enables current-controlled conversion of electrical energy to mechanical energy. Electrolysis does not involve any side reactions (Neagu 2000), making electrolysis efficient in terms of low heat generation. Some delay to forward flow during the current application period was present in all RIMS tested (no valve, two commercial valves, and one MEMS check valve) and was attributed to the compliant nature of the silicone reservoir and catheter, low current applied (Neagu 1998), and slow diffusion of hydrogen and oxygen gases away from the electrode (Böhm et al. 1999).

Recently, Nafion®-coating of Pt electrodes demonstrated great improvement in actuator efficiency, linearity, and repeatability (Sheybani and Meng 2011). Gases are more soluble in Nafion® than water, and therefore gases quickly diffuse away from the electrode to prevent bubble occlusion of the reaction sites. The coating also improves recombination, such that recombination can occur on the order of minutes. Future RIMS will employ Nafion®-coated actuators for even greater accuracy and reduced delays in pumping onset after current application.

For *in vivo* studies, preventing reverse flow is desired to prevent biological fluids from mixing with the drug from the reservoir. The commercial valves and our fabricated valve require a finite sealing pressure (> 6.89 kPa for one-way disc valve, >1.03 kPa or 7.76 mmHg for in-line check valve) which exceed that produced in RIMS, resulting in significant reverse flow during recombination. From these results it is clear that a valve with a much lower sealing pressure (no reverse leakage) is necessary for our system. Commercially available valves could not provide the desired performance and it remains a challenge to develop reliable MEMS check valves for this application; further research on check valves is required. Valved RIMS also experienced a slight delay to forward flow due to the added resistive element and pressure build up required to overcome the valve cracking pressure. However, the slopes of the curves for non-valved and commercially-valved RIMS were similar as the flow rate was coupled to gas generated by the applied constant current.

6 Application in cancer therapy

A potential application of the RIMS is for controlled, localized delivery of short half-life compounds *in vivo*, such as siRNA (Dykxhoorn et al. 2006). In preliminary studies, we demonstrated RIMS for subcutaneous delivery of anti-cancer drugs to tumors (Gensler et al. 2010). An siRNA-gold nanoplex drug (HNB-001) was developed that reduces radiation resistance in certain types of tumors expressing a gene for the protein sphingosine-kinase-1 (SPK-1), but lacked a suitable site-specific delivery method (Dykxhoorn et al. 2006; Gensler et al. 2010). HT29 cells were implanted subcutaneously in both sides of the flank of nude mice to induce tumors, with the left tumor receiving treatment and the right acting as a control with no treatment (Gensler et al. 2010). All procedures were performed in accordance with protocols approved by the University of Southern California's Institutional Animal Care and Use Committee. A RIMS with Pt-Ti electrodes on Parylene C (no valve) delivered the nanoplexes directly to the tumor site in mice under constant current of 0.78 mA. The RIMS (active pumps) delivered a bolus of ~50 µl daily for 2 weeks, with reservoir refills twice per week. Passive pumps were assembled and used to deliver control treatments: phosphate buffered saline, gold nanorods, free siRNA, and nanoplexes. These units did not contain an electrochemical bellows actuator or valve and consisted only of the silicone reservoir cavity and catheter. Without the actuator, these implanted pumps provided drug by diffusion from the reservoir through the catheter. Injections of phosphate buffered saline, free siRNA, and nanoplexes were also conducted at the same rate and with the same bolus volume as the RIMS. A subset of the treated tumors were exposed to 100 rad of radiation. The active delivery of nanoplexes by the RIMS in combination with radiation treatment showed significant tumor regression (~50%) over both diffusion and injection, with the greatest effect occurring adjacent to the catheter tip (Gensler et al. 2010).

7 Conclusions and future work

We developed a refillable implantable micropump system with great potential for a multitude of applications, from drug development to highly flexible pharmaceutical studies

in research animals as small as mice. We demonstrated the ability to administer drug to small animals with control over delivery rates and volume, with an example of chronic delivery of a novel gene therapy drug. We have shown preliminary success in using gene therapy in combination with radiation to combat cancerous tumors, and that active delivery was essential to this outcome. Our next steps include using Nafion®-coated actuators in RIMS to further improve repeatability of the micropump, using a rigid material for the reservoir to eliminate compliance, improved catheter designs to ensure optimal delivery to the site, and development of a valve with no reverse leakage. Future devices will be powered wirelessly, allowing the animals to move freely without tethers or wires and enabling a new paradigm in laboratory research with small animals.

Acknowledgements This work was supported in part by the Wallace H. Coulter Foundation Early Career Translational Research Award, National Institutes of Health/National Eye Institute under award number R21EY018490, and National Institutes of Health/National Institute on Drug Abuse under award number R21DA026970. H.G. was supported by a National Science Foundation Graduate Research Fellowship. The authors would like to thank Dr. Ken-Tye Yong, Dr. Indrajit Roy and Dr. Paras N. Prasad of University of Buffalo, The State University of New York, for providing the gold nanoparticles; Dr. Rizwan Masood and Dr. Uttam K. Sinha for providing the HNB-001 siRNA-gold nanoplexes and their surgical expertise; and Sutao Zhu of the University of Southern California for her surgical expertise. We would also like to thank Dr. Donghai Zhu and the members of the USC Biomedical Microsystems Laboratory for their assistance with this project.

References

Alzet. ALZET® Osmotic Pumps—Implantable pumps for research. Available at: http://www.alzet.com/ [Accessed October 19, 2011a]

J. Ambati et al., Transscleral delivery of bioactive protein to the choroid and retina. Investig Ophthalmol Vis Sci **41**(5), 1186–1191 (2000)

F. Amirouche, Y. Zhou, T. Johnson, Current micropump technologies and their biomedical applications. Microsyst Technol **15**, 647–666 (2009)

A. Bard, *Electrochemical methods: fundamentals and applications*, 2nd edn. (Wiley, New York, 2001)

C. Belmont, H.H. Girault, Coplanar interdigitated band electrodes for synthesis Part I: ohmic loss evaluation. J Appl Electrochem **24**, 475–480 (1994)

E. Benedikz, E. Kloskowska, B. Winblad, The rat as an animal model of Alzheimer's disease. J Cell Mol Med **13**, 1034–1042 (2009)

S. Böhm, W. Olthuis, P. Bergveld, An integrated micromachined electrochemical pump and dosing system. Biomed Microdevices **1**(2), 121–130 (1999)

Debiotech. Debiotech—Medical Devices—Switzerland. Available at: http://www.debiotech.com/ [Accessed November 18, 2011b]

D.M. Dykxhoorn, D. Palliser, J. Lieberman, The silent treatment: siRNAs as small molecule drugs. Gene Ther **13**(6), 541–552 (2006)

N. Elman et al., The next generation of drug-delivery microdevices. Clin Pharmacol Ther **85**(5), 544–547 (2009)

A.T. Evans, S. Chiravuri, Y.B. Gianchandani, A multidrug delivery system using a piezoelectrically actuated silicon valve manifold with embedded sensors. J Microelectromechanical Syst **20**, 231–238 (2011)

O.C. Farokhzad, R. Langer, Impact of nanotechnology on drug delivery. ACS Nano **3**, 16–20 (2009)

F. Faupel, R. Willecke, A. Thran, Diffusion of metals in polymers. Mater Sci Eng R Rep **22**(1), 1–55 (1998)

H. Gensler et al., Implantable MEMS drug delivery device for cancer radiation reduction. In *Proc. IEEE Int. Conf. MEMS*, (IEEE Int. Conf. MEMS, Hong Kong, SAR, China, 2010), pp. 23–26

H. Gensler, R. Sheybani, E. Meng, Rapid non-lithography based fabrication process and characterization of Parylene C bellows for applications in MEMS electrochemical actuators. In *Proc. IEEE Int. Conf. TRANSDUCERS*, (IEEE Int. Conf. TRANSDUCERS, Beijing, China, 2011), pp. 2347–2350

A.C.R. Grayson et al., Multi-pulse drug delivery from a resorbable polymeric microchip device. Nat Mater **2**, 767–772 (2003)

iPrecio. iPRECIO®, Innovative Drug Infusion Technology for Laboratory Animals. Available at: http://www.iprecio.com/ [Accessed October 19, 2011c]

J.W., Judy, T. Tamagawa, D.L., Polla, Surface-machined micromechanical membrane pump. In *Proc. IEEE Int. Conf. MEMS* IEEE Int. Conf. MEMS, (IEEE, Nara, Japan, 1991), pp. 182–186

I.O. K'Owino, O.A. Sadik, Impedance spectroscopy: a powerful tool for rapid biomolecular screening and cell culture monitoring. Electroanalysis **17**, 2101–2113 (2005)

K. Kramer et al., The use of radiotelemetry in small laboratory animals: recent advances. Contemp Topics Lab Anim Sci / Am Assoc Lab Anim Sci **40**(1), 8–16 (2001)

D.J. Laser, J.G. Santiago, A review of micropumps. J Micromech Microeng **14**, R35–R64 (2004)

L.-H. Lee, *Fundamentals of adhesion* (Plenum Press, New York, 1991)

J.H. Lee et al., Microstructure and adhesion of Au deposited on Parylene-c substrate with surface modification for potential immunoassay application. IEEE Trans Plasma Sci **32**, 505–509 (2004)

P.-Y. Li, *Implantable bioMEMS drug delivery systems. Ph.D. Dissertation* (Dept. Biomed. Eng., University of Southern California, Los Angeles, 2009)

Y. Li et al., In vivo release from a drug delivery MEMS device. J Control Release **100**(2), 211–219 (2004)

P.-Y. Li et al., An electrochemical intraocular drug delivery device. Sens Actuators A Phys **143**(1), 41–48 (2008)

P.-Y. Li, et al., A Parylene bellows electrochemical actuator for intraocular drug delivery, in *Proc. IEEE Int. Conf. TRANSDUCERS*, (IEEE Int. Conf. TRANSDUCERS, Denver, CO, USA, 2009), pp. 1461–1464

P.-Y. Li et al., A Parylene bellows electrochemical actuator. J Microelectromechanical Syst **19**(1), 215–228 (2010)

R. Lo, E. Meng, A modular heat-shrink-packaged check valve with high pressure shutoff. J Microelectromechanical Syst **20**, 1163–1173 (2011)

R. Lo, E. Meng, In-plane Bandpass Regulation Check Valve in Heat-Shrink Packaging for Drug Delivery. In *Proc. IEEE Int. Conf. MEMS*. (IEEE Int. Conf. MEMS, Sorrento, Italy, 2009), pp. 236–239

R. Lo et al., A passive MEMS drug delivery pump for treatment of ocular diseases. Biomed Microdevices **11**, 959–970 (2009)

D. Maillefer et al., A high-performance silicon micropump for an implantable drug delivery system, in *Proc. IEEE Int. Conf. MEMS*. IEEE Int. Conf. MEMS, (IEEE, Orlando, FL, USA, 1999), pp. 541–546

D. Maillefer et al., A high-performance silicon micropump for disposable drug delivery systems, in *Proc. IEEE Int. Conf. MEMS*. IEEE Int. Conf. MEMS. Interlaken, (IEEE, Switzerland, 2001), pp. 413–417

Med-e-Cell. Welcome to Med-e-Cell: infusion pumps, fluid delivery devices, oxygen generation/control and fuel cell technology for licensing and development partnerships. Available at: http://medecell.com/ [Accessed October 19, 2011d]

E. Meng, P.-Y. Li, Y.-C. Tai, A biocompatible Parylene thermal flow sensing array. Sens Actuators A Phys **144**, 18–28 (2008)

C.R. Neagu, *A Medical Microactuator based on an Electrochemical Principle* (University of Twente, Entschede, 1998)

C.R. Neagu, The electrolysis of water: an actuation principle for MEMS with a big opportunity. Mechatronics **10**, 571–581 (2000)

C.R. Neagu et al., An electrochemical microactuator: principle and first results. J Microelectromechanical Syst **5**, 2–9 (1996)

N.T. Nguyen, X. Huang, T.K. Chuan, MEMS-micropumps: a review. J Fluids Eng **124**(2), 384–392 (2002)

A. Parthasarathy, The platinum microelectrode/Nafion interface: an electrochemical impedance spectroscopic analysis of oxygen reduction kinetics and Nafion characteristics. J Electrochem Soc **139**, 1634 (1992)

S. Petit-Zeman, Rat genome sequence reignites preclinical model debate. Nat Rev Drug Discov **3**, 287–288 (2004)

X. Ruan, Drug-related side effects of long-term intrathecal morphine therapy. Pain Physician **10**(2), 357–366 (2007)

J.T. Santini Jr. et al., Microchips as controlled drug-delivery devices. Angew Chem Int Ed **39**, 2396–2407 (2000)

D. Sawyer, *Experimental electrochemistry for chemists* (Wiley, New York, 1974)

R. Sheybani, E. Meng, High efficiency wireless electrochemical actuators: Design, fabrication and characterization by electrochemical impedance spectroscopy, in *Proc. IEEE Int. Conf. MEMS*. (IEEE Int. Conf. MEMS, Cancun, Mexico, 2011), pp. 1233–1236

R. Sheybani, H. Gensler, E. Meng, Rapid and repeated bolus drug delivery enabled by high efficiency electrochemical bellows actuators, in *Proc. IEEE Int. Conf. TRANSDUCERS*. IEEE Int. Conf. TRANSDUCERS, (IEEE, Beijing, China, 2011), pp. 490493

J.G. Smits, Piezoelectric micropump with microvalves, in *Proc. University/Government/Industry Microelectronics Symposium*. University/Government/Industry Microelectronics Symposium, (IEEE 1989), pp. 92–94

M.H. Smolensky, N.A. Peppas, Chronobiology, drug delivery, and chronotherapeutics. Adv Drug Deliv Rev **59**(9–10), 828–851 (2007)

M. Staples, Microchips and controlled-release drug reservoirs. Wiley Interdiscip Rev Nanomedicine Nanobiotechnology **2**, 400–417 (2010)

F.L. Trull, B.A. Rich, More regulation of rodents. Science **284**, 1463 (1999)

N.C. Tsai, C.Y. Sue, Review of MEMS-based drug delivery and dosing systems. Sens Actuators A Phys **134**(2), 555–564 (2007)

J. Urquhart, J.W. Fara, K.L. Willis, Rate-controlled delivery systems in drug and hormone research. Annu Rev Pharmacol Toxicol **24**, 199–236 (1984)

A.V. Vasenkov, Atomistic modeling of Parylene-metal interactions for surface micro-structuring. J Mol Model **17**(12), 3219–3228 (2011)

P. Woias, Micropumps–past, progress and future prospects. Sens Actuators B Chem **105**(1), 28–38 (2005)

K.C. Worley, G.M. Weinstock, R.A. Gibbs, Rats in the genomic era. Physiol Genomics **32**, 273–282 (2007)

P.K. Wu et al., Metal/polymer interface adhesion by partially ionized beam deposition. J Appl Phys **80**, 5759 (1996)

B.B. Youan, Chronopharmaceutics: gimmick or clinically relevant approach to drug delivery? J Control Release **98**(3), 337–353 (2004)

K.-S. Yun, E. Yoon, Micropumps for MEMS/NEMS and Microfluidic Systems, in *MEMS/NEMS*, ed. by C.T. Leondes (Springer US, Boston, 2006), pp. 1112–1144

R. Zengerle, A. Richter, H. Sandmaier, A micro membrane pump with electrostatic actuation, in *Proc. IEEE Int. Conf. MEMS*. IEEE Int. Conf. MEMS. Travemunde, (IEEE, Germany, 1992), pp. 19–24